Optimizing Nanoplasmonic Biosensor Sensitivity with Orientated Single Domain Antibodies

Marc P. Raphael[1] · Joseph A. Christodoulides[1] · Jeff M. Byers[1] ·
George P. Anderson[2] · Jinny L. Liu[2] · Kendrick B. Turner[2] ·
Ellen R. Goldman[2] · James B. Delehanty[2]

Abstract Localized surface plasmon resonance (LSPR) spectroscopy and imaging are emerging biosensor technologies which tout label-free biomolecule detection at the nanoscale and ease of integration with standard microscopy setups. The applicability of these techniques can be limited by the restrictions that surface-conjugated ligands must be both sufficiently small and orientated to meet analyte sensitivity requirements. We demonstrate that orientated single domain antibodies (sdAb) can optimize nanoplasmonic sensitivity by comparing three anti-ricin sdAb constructs to biotin-neutravidin, a model system for small and highly orientated ligand studies. LSPR imaging of electrostatically orientated sdAb exhibited a ricin sensitivity equivalent to that of the biotinylated LSPR biosensors for neutravidin. These results, combined with the facts that sdAb are highly stable and readily produced in bacteria and yeast, build a compelling case for the increased utilization of sdAbs in nanoplasmonic applications.

Keywords LSPR · SPR · Single domain antibodies ·
Orientation · Ricin · Bio-threat

✉ Marc P. Raphael
marc.raphael@nrl.navy.mil

1   Bioelectronics and Sensing, Code 6363, Naval Research Laboratory,
4555 Overlook Ave SW, Washington, DC 20375, USA

2   Center for Bio/Molecular Science and Engineering, Code 6900,
Naval Research Laboratory, 4555 Overlook Ave SW,
Washington, DC 20375, USA

Introduction

Localized surface plasmon resonance (LSPR) biosensing is a label-free technique that enables biomolecule detection with nanoscale spatial resolution. Since its introduction, the technique has found a broad range of applications including studies of DNA-protein interactions [1], toxins [2], proteins [3, 4], and vesicles [5]. The small size of the individual sensors, typically 40 to 150 nm in diameter, has the potential to enable sensor miniaturization to a scale unapproachable by the closely related planar technique of surface plasmon resonance (SPR) biosensing. Also unique to LSPR is that the nanoplasmonic resonance condition is satisfied in a simple reflected or transmitted light geometry, common to both microscopy and spectroscopy applications, whereas SPR excitation requires incident light that is totally internally reflected. As a result, LSPR spectroscopy and imaging (LSPRi) are increasingly being integrated into live-cell microscopy experiments for the detection of secreted proteins while simultaneously imaging the cells with more traditional techniques such as fluorescence and bright field [6–9].

Continued progress in the field of nanoplasmonic biosensing is highly dependent upon meeting two design challenges related to surface functionalization. First, the reduced sensor area limits the number of conjugated ligands, making orientation critical for maximizing the probability of analyte capture. The most common ligands in biosensing are full antibodies, surface conjugated via their lysine residues or N-terminal amino groups. The typical antibody will have 60–80 of such residues resulting in a range of surface orientations, many of which are not optimal for analyte detection [10]. Second, experimental evidence and theoretical models show the nanostructures can exhibit a wide range of electromagnetic field decay lengths into the solution with some as short as 5 to 15 nm [11, 12]. Such nanoscale distances are largely filled

 Springer

when using intact IgG antibodies that have typical dimensions of 14.5 nm×8.5 nm×4.0 nm [13]. As a result, LSPR optimization requires at a minimum highly oriented full antibodies as ligands [14] and preferably lower molecular weight molecules which can be modified to enhance preferential orientation.

There are a number of classes of biomolecules which have been engineered with the goal of meeting these criteria including single chain antibodies (ScFvs), Fab fragments, and aptamers. Orientated ScFvs, which are roughly one fifth the size of full antibodies, were recently shown to enhance LSPR sensitivity relative to whole antibody counterparts [15]. In general, however, attempts to orient ScFvs and Fab fragments for improved biosensor sensitivity have produced decidedly mixed results [16–22, 10]. In addition, ScFvs and Fab fragments with molecular weights of approximately 27 and 50 kDa, respectively, are still relatively large ligands for many LSPR biosensing applications, leaving room for improved sensitivity if the size can be further reduced.

Single domain antibodies (sdAb), also called nanobodies, are the recombinant variable domain derived from heavy chain-only antibodies found in camelids, i.e., camels, llamas, and alpacas. Consisting of only a single domain endows sdAb with a number of attractive properties for biosensor applications. First, their small size (~15 kDa or ~1/10 the size of a full IgG) allows for facile production in yeast or bacteria, alone or as fusions with effector proteins. Second, both their small size and being a single domain provides them with remarkable thermostability, being able to refold and recover their binding ability following heat or chemical denaturation. Finally, sdAb are derived from true antibodies; thus, they possess the high affinity and specificity for which antibodies are renowned. SdAb, which recognize a plethora of targets, have been developed, and orientated sdAb have recently been demonstrated to improve SPR biosensor sensitivity [23, 24]. Our primary focus has been on the development of robust reagents for the detection of bio-threat agents [25, 26]. Of those reagents, the sdAb which bind ricin have been the most studied, and thus make well defined tools for testing the utility of sdAb in novel sensor applications [27, 28].

Here, we compare the sensitivity of LSPRi for orientated versus randomly surface-conjugated sdAb. Using anti-ricin sdAb, we first demonstrate the ability to modify the carboxyl terminus with positively charged peptide tails and rhizavidin fusion proteins for preferential surface orientation. The positively charged tail was designed to aid in surface orientation by means of an electrostatic interaction with a negatively charged surface. The rhizavidin fusion construct was designed to assist in orientation by binding to a biotinylated surface, preferentially directing the sdAb into the solution. Using SPR imaging (SPRi), we show that these modified sdAb have enhanced surface conjugation efficiencies and improved sensitivity to ricin relative to the non-orientated sdAb. We then measured the sdAb sensitivity to ricin on an LSPRi platform

and compared the results to the biotin-neutravidin binding pair, a commonly used standard for biosensing applications and an apt comparison since biotin is readily orientated and ricin and neutravidin have similar molecular weights [3, 29]. Despite the fact that the sdAb ligands were 62-fold greater in mass than biotin, the measured sensitivities were statistically equivalent. We conclude that the relatively small size and the ability to readily modify sdAb for orientated surface conjugation make them optimal ligand candidates for LSPR imaging and spectroscopy applications. The current sensitivity study lays the groundwork for future work in determining the LSPRi limit of detection of each construct and multiplexed toxin-sensing applications.

Experimental

The sequence and binding characteristics of the ricin-binding sdAb C8 and D12 have been previously described [27, 28]; both have sub-nM affinity for the toxin ricin. The clone D12f is a version of D12 in which an unpaired cysteine was mutated to a serine causing no change in sdAb affinity. The C8 sdAb, lacking the upper hinge region, was cloned into pET22b for protein expression. Protein was purified using immobilized metal affinity chromatography followed by size exclusion chromatography on an FPLC as previously described [26, 30]. Protein sequences of all sdAb constructs are detailed in the Supplementary Material.

The construct referred to herein as C8-zip is a genetic fusion of the C8 sdAb with a positively charged leucine zipper described by Oshea et al. [31]. DNA including a glycine-serine linker followed by the zipper sequences was synthesized by GenScript (Piscataway, NJ) and included flanking Not I and Xho I restriction endonuclease sites. We cloned the linker-zipper sequence into pET22b and then mobilized the C8 sdAb into the modified pET22b through the Nco I and Not I sites; DNA sequencing was used to confirm the constructs. Protein was produced from the periplasmic space in a protocol identical to that used to purify C8. This C8-Zip construct had initially been prepared to facilitate sdAb heterodimer formation [32].

The D12f-rhiz construct is a genetic fusion of the D12f sdAb with the biotin binding protein rhizavidin (rhiz). Unlike our previously described sdAb-rhiz fusion construct, the D12f-rhiz does not include the upper hinge sequence between the D12f and rhiz. Protein production was as described for our previous sdAb-rhiz fusions [33].

Details of the LSPR chip fabrication and the LSPRi measurement setup have been published previously [34, 29]. In short, square arrays of gold nanostructures were patterned on No. 1.5 glass coverslips using electron-beam nanolithography (Raith GmbH) to expose a bilayer resist structure consisting of polymethyl methacrylate and ethyl lactate methyl

methacrylate copolymer purchased from Microchem Corp. Each array measured 6 μm × 6 μm and consisted of 400 evenly spaced nanostructures separated by a pitch of 300 nm. The bases of the nanostructures were circular in cross section with diameters of 70±5 nm and the heights were 75±2 nm, giving a plasmonic resonance peak centered at ∼635 nm in 10 mM phosphate buffered saline (Thermo Scientific). Protein binding to the Au surface creates a perturbation in the local index of refraction which induces a redshift in the resonance peak as well as enhanced scattering. In the LSPRi measurement, this response is manifested as an increase in the nanoplasmonic array's brightness as imaged by the camera. We have shown, using analytes such as neutravidin and IgG proteins, that this response can be calibrated to the fractional occupancy of surface-bound receptors. Commercial SPRi has sensors that are orders of magnitude larger in surface area but operates on a similar physical principle. When using the same functionalization chemistries, results from the two techniques can be correlated [8, 34].

The chip was loaded onto a custom-built microfluidic assembly consisting of a 300-μL chamber to which the analyte solution was introduced using a peristaltic pump from Instech Laboratories (P720). All imagery was acquired using Zeiss Zen software, an inverted Zeiss Axio Observer microscope, a 40X/1.4 NA objective, and a thermoelectrically cooled 16-bit sCMOS camera from Hamamatsu (Flash 4.0) operated in 2×2 binning mode. Images were collected in a reflected light geometry using Koehler illumination, a 100 W halogen lamp, and crossed polarizers to reduce the collection of light scattered from the substrate. Error bars in the LSPRi response represent the standard deviation from nine averaged arrays. Unless otherwise shown, the error bars are within the size of the data markers.

SPRi measurements were conducted with Bio-Rad's XPR36 protein analysis system, the sensors of which consisted of a gold thin film deposited atop a glass prism for excitation of surface plasmon polaritons by total internal reflection. Once inserted into the instrument, each chip is microfluidically arrayed into 36 measurement spots. This enabled a range of sdAb ligands to be functionalized on a single chip in contrast to the LSPRi setup in which each experiment consisted of only one ligand type. All LSPRi and SPRi measurements were conducted at 25 °C. Error bars in the SPR response are the standard deviation from averaging five measurement spots on the same chip. Unless otherwise shown, the error bars are within the size of the data markers.

For SPRi studies of sdAb, the Bio-Rad chips were cleaned down to the bare gold surface by RF plasma ashing at 40 W in 300 mTorr of a 5 % hydrogen, 95 % argon mixture, and then functionalized with a two-component self-assembled monolayer (SAM) by immersion for 18 h in an ethanolic-based thiol solution (0.5 mM), consisting of a 3:1 ratio of SH-$(CH_2)_8$-EG_3-OH (SPO) to SH-$(CH_2)_{11}$-EG_3-COOH (SPC)

(Prochimia Surfaces Sp.) for C8 and C8-zip studies. The chips were then rinsed with EtOH and dried under flowing nitrogen gas. Activation of the SPC component consisted of introducing a 33 mM: 133 mM ratio of N-hydroxysulfosuccinimide (sulfo-NHS) and 1-ethyl-3-[3-dimethylaminopropyl]carbodiimide hydrochloride (EDC) from Thermo Scientific in ultrapure water (DDW; EMD Millipore) for 5 min at a flow rate of 30 μL/min. This was followed by a 5-min rinse with DDW and the introduction of the sdAb under the range of concentration and pH conditions described in the "Results and Discussion" section. For the D12f-rhiz studies, a 2-mg/mL solution of (+)-biotinyl-3,6-dioxaoctanediamine (amine-PEG_2-biotin) from Thermo Scientific was introduced over the activated surface at 30 μL/min for 5 min followed by a range of D12f-rhiz concentrations as described in the "Results and Discussion" and Supplementary Material sections. Finally, in all cases, unreacted –COOH groups were blocked by flowing 0.1 M ethanolamine (Bio-Rad) in PBS for 5 min at 30 μL/min. For the LSPR chips, this process was repeated except all solutions were manually drop coated and washed while inside the custom-built microfluidic assembly.

The identical surface cleaning and SAM layer formation protocol was applied for LSPRi biotin-neutravidin studies except that the two-component SAM layer consisted of a 3:1 ratio of SH-$(CH_2)_8$-EG_3-OH (SPO) to SH-$(CH_2)_{11}$-EG_3-NH_2 (SPN) (Prochimia Surfaces Sp.). LSPR chips were drop coated with 100 μL of 2 mg/mL sulfo-NHS-biotin (Thermo Scientific) in PBS, incubated for 30 min at room temperature, rinsed with DDW, and dried in flowing nitrogen.

Results and Discussion

Three ligands were used in this study: an unmodified sdAb (C8), a genetic fusion of C8 with a positively charged peptide (C8-zip), and a genetic fusion of the D12f sdAb with the biotin binding protein rhizavidin (D12f-rhiz). Both the C8 and D12f sdAb that compose the ligand provide the recognition function of the constructs and are specific for ricin. They bind the same epitope on the toxin and exhibit nearly identically sub-nM affinities for their cognate antigen. Structurally, the binding loops of sdAb are located on the opposite side from their C-terminus, enabling the construction of fusions to facilitate directional immobilization. We hypothesized that the positively charged lysines on the C-terminus of C8-zip protein would maximize the potential for directional immobilization on the negatively charged –COOH surface, resulting in an orientation with the tail coupled to the surface and the binding region oriented into solution for optimal antigen capture. In a similar way, the D12f-rhiz enables directional immobilization but via the biotinylated surface [33].

To optimize the plasmonic sensitivity to ricin, a range of ligand concentrations were introduced over the EDC/Sulfo-NHS activated SPR surface followed by a saturating concentration of ricin (100 nM). Fig. 1a shows the SPR response to C8-zip in which the concentration was varied from 0.4 to 30 μg/mL in PBS, pH 7.0. At the higher ligand concentrations, there were diminishing returns with regards to ricin-binding capacity (Fig. 1b) with the 30 μg/mL exposed surface binding only 8 % more than the surface coated at 10 μg/mL. Exceeding this 30 μg/mL value resulted in a rapid increase in non-specific binding and minimal ricin sensitivity enhancement. C8 and D12f-rhiz exhibited similar surface saturation concentrations, lying between 1 and 30 μg/mL (Supplementary Material). Ligand concentration values such as the 30 μg/mL value for C8-zip were defined as optimal based on these criteria of maximizing sensitivity and minimizing non-specific binding. A control study was also conducted in which a 100-nM ricin solution was first incubated with 5 μM of C8 for 45 min to block the ricin-binding sites. When the blocked ricin was introduced over a C8-functionalized surface, no response was detectable, demonstrating levels of non-specific binding below the SPRi limit of detection (Fig. 1b).

A study was then conducted of SPR sensitivity to ricin at each ligand's optimal concentration. The 36-array microfluidic architecture of the XPR36 allowed for these measurements to be taken simultaneously alongside control lanes, thus eliminating uncertainties from chip-to-chip variations. C8-zip exhibited the highest response to 100 nM ricin, 320 % higher than that of C8 and 42 % higher than that of D12f-rhiz (Fig. 2a). In order to help isolate sensitivity improvements due to ligand orientation, we next introduced ricin over C8 and C8-zip surfaces prepared with similar ligand responses (1300±120 RU) which is indicative of equivalent ligand surface densities. Figure 2b shows the SPR response to 100 nM ricin for these surface conjugations. The C8-zip surface again exhibited the highest response to 100 nM ricin, 140 % higher than that of C8.
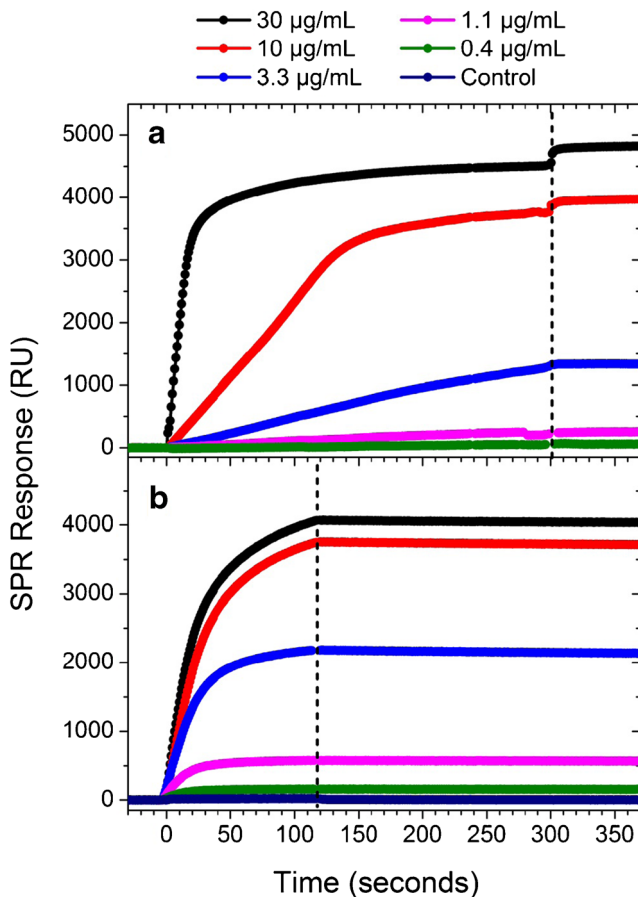
Fig. 1 a SPR response to the conjugation of C8-zip sdAbs for a range of ligand concentrations followed by the introduction of 100 nM ricin in (b). The control study in b consisted of a 100-nM ricin solution incubated with 5 μM of C8 for 45 min to block the binding sites. It was then introduced over a 4.0-μg/mL C8 functionalized surface. The vertical dashed line separates the association phase (left) in which the ligand or analyte solution is flowing over the surface from the dissociation phase (right) in which buffer flows over the surface
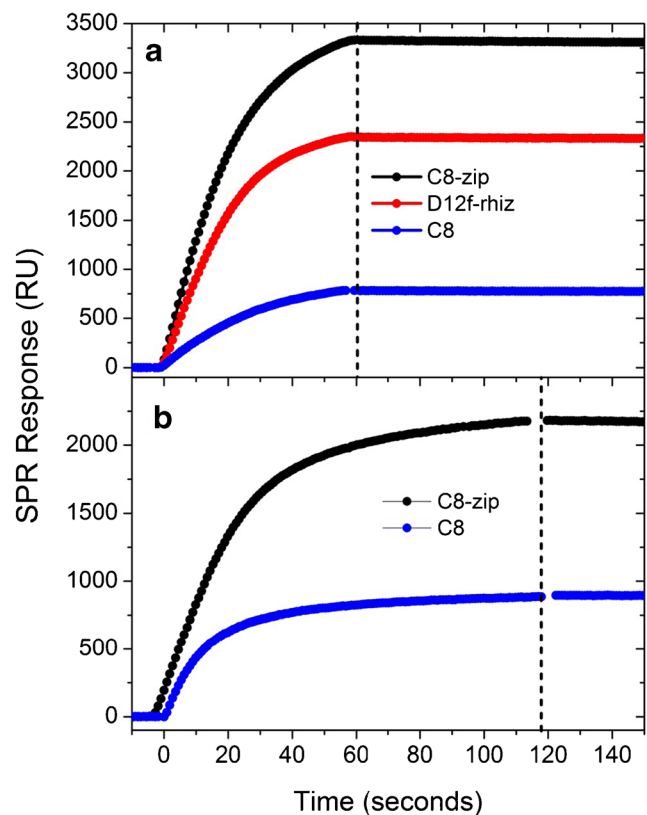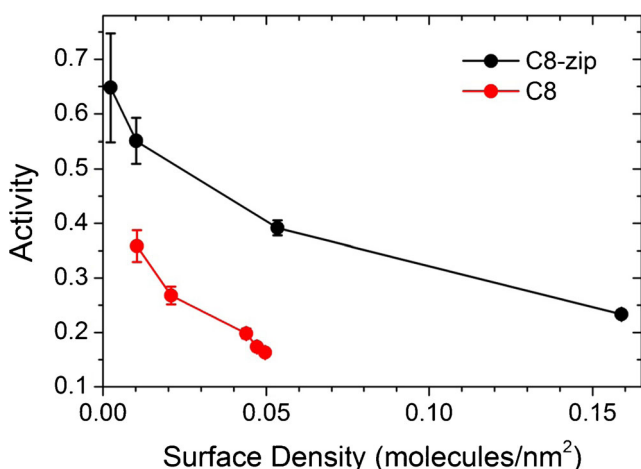
Fig. 2 a SPR response to 100 nM ricin of optimally prepared C8-zip, C8, and D12f-rhiz surfaces. b SPR analyte response to 100 nM ricin following C8-zip and C8 ligand conjugations with responses of 1300± 120 RU. Measurements were conducted in parallel by multiplexing a single sensor chip to eliminate chip-to-chip variations. The vertical dashed line separates the association phase (left) in which the analyte solution is flowing over the surface from the dissociation phase (right) in which buffer flows over the surface

To further investigate relative ligand orientation, we compared the analyte binding activity, A, of the conjugated C8 and C8-zip ligands, defined as the moles of captured analyte divided by the moles of surface-conjugated ligand. In SPR, the moles of a given molecule deposited on the surface is proportional to the instrument response, X, divided by the molecular weight, m, so that the activity is readily expressed as

$$A = \frac{X_A \cdot m_L}{X_L \cdot m_A}$$

where X_L and X_A are the SPR responses in RU to the binding of ligand and analyte, respectively, m_L and m_A are the molecular weights of the ligand and analyte, respectively, and it is assumed that the ligands are monovalent.

To properly isolate the effect of orientation on A, care must be taken to work in the dilute ligand limit in order to minimize steric hindrance effects. If analyte molecules can repel one another at the surface, the result is a reduced activity value unrelated to ligand orientation. Figure 3 compares the activity of C8-zip to C8 for a range of surface ligand densities by exposing the surface to ligand concentrations of 0.25 to 10 µg/mL for 300 s. The ligand surface density was calculated assuming a sensor calibration of 1 RU=1 pg/mm^2 [35]. At higher surface densities, the activity values of the two ligands converge as expected for a surface dominated by steric hindrance. As the surface concentration is reduced, both exhibit marked increases with maximum C8-zip and C8 activities of 65 and 36 %, respectively. The results indicate that the positively charged tail of the C8-zip improved surface orientation and are consistent with the enhanced sensitivity measured in Fig. 2. We also observed improved sensitivity for the orientated sdAb when using SPR GLC sensor chips, designed by Bio-Rad for general amine coupling via a compact polymer layer with a binding capacity of approximately one protein monolayer (Supplementary Material).

For the corresponding nanoplasmonic response studies, a functionalization protocol identical to that used for the SPR study in Fig. 2a was applied to the gold nanostructures of the custom-made LSPR chips. Response data to 100 nM ricin were determined by averaging the mean intensity of nine arrays, each array consisting of 400 nanostructures (Fig. 4a, b). As with the SPR results, the C8-zip surface was the most sensitive of the three ligands, with a saturation response that was 104 % greater than that of C8 and 61 % greater than that of D12f-rhiz (Fig. 4c).

To further characterize the sensitivity of the C8-zip functionalized surface, we conducted LSPRi studies in which the surface was functionalized with biotin and exposed to a 100-nM neutravidin solution, a commonly used standard in nanosensor characterization. Both of these receptor-ligand pairs have exceptionally high binding affinities and both ricin and neutravidin have approximately the same molecular weight (60 kDa). Biotin, however, is readily orientated and has a molecular weight of 244 Da, 62 times lower than that of C8-zip. Thus, the differences in LSPRi sensitivity to analyte should be reflective of ligand size and degree of orientation.
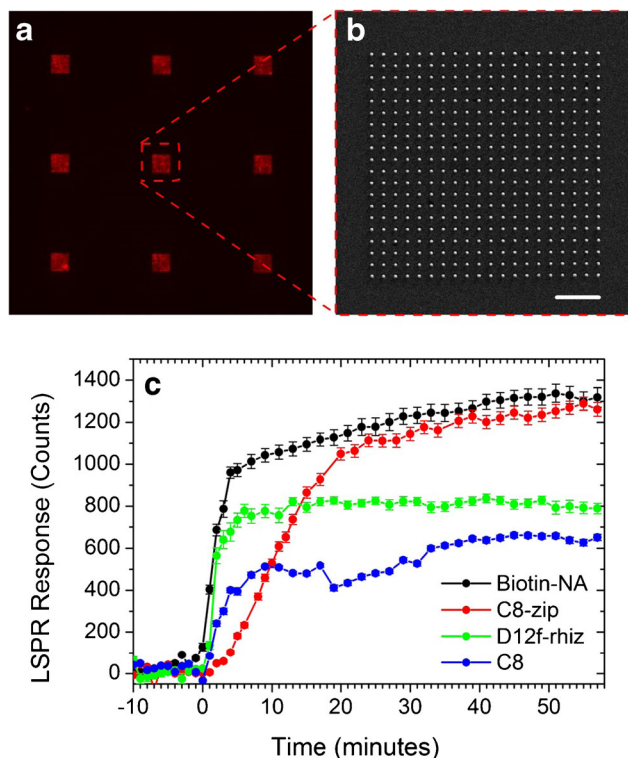
Fig. 4 **a** LSPRi of nine arrays, each array consisting of 400 nanostructures. The image is false colored *red* to indicate the resonance wavelength of 635 nm. **b** Scanning electron microscopy of an array of 400 nanostructures. **c** LSPRi response to 100 nM ricin for C8-zip, C8, and D12f-rhiz surfaces compared to that of a biotinylated surface for 100 nM neutravidin

Fig. 3 Ricin saturation activity versus ligand surface density for C8-zip and C8. Ligand surface density was calculated assuming a sensor calibration of 1 RU=1 pg/mm^2. The ricin concentration was 100 nM for all experiments

Interestingly, Fig. 4c shows the responses of the C8-zip and biotinylated surfaces to their cognate analytes were statistically equivalent, demonstrating that the small size and highly oriented conjugation of the C8-zip molecules are well suited for LSPRi applications. Future work will build on these results to estimate the limit of detection for each construct.

Conclusions

When conjugated to plasmonic nanostructures, orientated sdAb exhibited enhanced LSPRi sensitivity which matched that of biotinylated surfaces to neutravidin, long considered a model system for small and orientated ligand studies. The additional facts that sdAb produce well in bacteria and yeast, are readily modified, and robust to denaturation make them well suited for a broad range of SPR and LSPR biosensing applications. The application of LSPRi to ricin detection is an important step forward in the design of small, readily deployable biosensors against bio-threat agents.

References

1. Endo T, Kerman K, Nagatani N, Takamura Y, Tamiya E (2005) Label-free detection of peptide nucleic acid-DNA hybridization using localized surface plasmon resonance based optical biosensor. Anal Chem 77(21):6976–6984. doi:10.1021/ac0513459

2. Park JH, Byun JY, Mun H, Shim WB, Shin YB, Li T, Kim MG (2014) A regeneratable, label-free, localized surface plasmon resonance (LSPR) aptasensor for the detection of ochratoxin A. Biosens Bioelectron 59:321–327. doi:10.1016/j.bios.2014.03.059

3. Haes AJ, Van Duyne RP (2002) A nanoscale optical biosensor: sensitivity and selectivity of an approach based on the localized surface plasmon resonance spectroscopy of triangular silver nanoparticles. J Am Chem Soc 124(35):10596–10604. doi:10.1021/ja020393x

4. Sepulveda B, Angelome PC, Lechuga LM, Liz-Marzan LM (2009) LSPR-based nanobiosensors. Nano Today 4(3):244–251. doi:10.1016/j.nantod.2009.04.001

5. Dahlin AB, Jonsson MP, Hook F (2008) Specific self-assembly of single lipid vesicles in nanoplasmonic apertures in gold. Adv Mater 20(8):1436. doi:10.1002/adma.200701697

6. Endo T, Yamamura S, Kerman K, Tamiya E (2008) Label-free cell-based assay using localized surface plasmon resonance biosensor. Anal Chim Acta 614(2):182–189. doi:10.1016/j.aca.2008.03.022

7. Oh BR, Huang NT, Chen WQ, Seo JH, Chen PY, Cornell TT, Shanley TP, Fu JP, Kurabayashi K (2014) Integrated nanoplasmonic sensing for cellular functional immunoanalysis using human blood. ACS Nano 8(3):2667–2676. doi:10.1021/nn406370u

8. Raphael MP, Christodoulides JA, Delehanty JB, Long JP, Byers JM (2013) Quantitative imaging of protein secretions from single cells in real time. Biophys J 105(3):602–608. doi:10.1016/j.bpj.2013.06.022

9. Wang S, Ota S, Guo B, Ryu J, Rhodes C, Xiong Y, Kalim S, Zeng L, Chen Y, Teitell MA, Zhang X (2011) Subcellular resolution mapping of endogenous cytokine secretion by nano-plasmonic-resonator sensor array. Nano Lett 11(8):3431–3434. doi:10.1021/nl2018838

10. Wimalasena RL, Wilson GS (1991) Factors affecting the specific activity of immobilized antibodies and their biologically-active fragments. J Chromatogr Biomed Appl 572(1–2):85–102. doi:10.1016/0378-4347(91)80475-r

11. Haes AJ, Zou SL, Schatz GC, Van Duyne RP (2004) A nanoscale optical biosensor: the long range distance dependence of the localized surface plasmon resonance of noble metal nanoparticles. J Phys Chem B 108(1):109–116. doi:10.1021/jp0361327

12. Rindzevicius T, Alaverdyan Y, Kall M, Murray WA, Barnes WL (2007) Long-range refractive index sensing using plasmonic nanostructures. J Phys Chem C 111(32):11806–11810. doi:10.1021/jp072564w

13. Bagci H, Kohen F, Kuscuoglu U, Bayer EA, Wilchek M (1993) Monoclonal anti-biotin antibodies simulate avidin in the recognition of biotin. FEBS Lett 322(1):47–50. doi:10.1016/0014-5793(93)81108-c

14. Soler M, Estevez MC, Alvarez M, Otte MA, Sepulveda B, Lechuga LM (2014) Direct detection of protein biomarkers in human fluids using site-specific antibody immobilization strategies. Sensors 14(2):2239–2258. doi:10.3390/s140202239

15. Byun JY, Shin YB, Li T, Park JH, Kim DM, Choi DH, Kim MG (2013) The use of an engineered single chain variable fragment in a localized surface plasmon resonance method for analysis of the C-reactive protein. Chem Commun 49(82):9497–9499. doi:10.1039/c3cc45046e

16. Bonroy K, Frederix F, Reekmans G, Dewolf E, De Palma R, Borghs G, Declerck P, Goddeeris B (2006) Comparison of random and oriented immobilisation of antibody fragments on mixed self-assembled monolayers. J Immunol Methods 312(1–2):167–181. doi:10.1016/j.jim.2006.03.007

17. Chen HX, Huang JY, Lee J, Hwang S, Koh K (2010) Surface plasmon resonance spectroscopic characterization of antibody orientation and activity on the calixarene monolayer. Sens Actuators B 147(2):548–553. doi:10.1016/j.snb.2010.03.033

18. Lu B, Xie JM, Lu CL, Wu CG, Wei Y (1995) Oriented immobilization of Fab' fragments on silica surfaces. Anal Chem 67(1):83–87. doi:10.1021/ac00097a014

19. Shen ZH, Yan HP, Zhang Y, Mernaugh RL, Zeng XQ (2008) Engineering peptide linkers for scFv immunosensors. Anal Chem 80(6):1910–1917. doi:10.1021/ac7018624

20. Torrance L, Ziegler A, Pittman H, Paterson M, Toth R, Eggleston I (2006) Oriented immobilisation of engineered single-chain antibodies to develop biosensors for virus detection. J Virol Methods 134(1–2):164–170. doi:10.1016/j.jviromet.2005.12.012

21. Trilling AK, Beekwilder J, Zuilhof H (2013) Antibody orientation on biosensor surfaces: a minireview. Analyst 138(6):1619–1627. doi:10.1039/c2an36787d

22. Vareiro MLM, Liu J, Knoll W, Zak K, Williams D, Jenkins ATA (2005) Surface plasmon fluorescence measurements of human chorionic gonadotrophin: role of antibody orientation in obtaining

enhanced sensitivity and limit of detection. Anal Chem 77(8): 2426–2431. doi:10.1021/ac0482460

23. Trilling AK, Hesselink T, van Houwelingen A, Cordewener JHG, Jongsma MA, Schoffelen S, van Hest JCM, Zuilhof H, Beekwilder J (2014) Orientation of llama antibodies strongly increases sensitivity of biosensors. Biosens Bioelectron 60:130–136. doi:10.1016/j.bios.2014.04.017

24. Walper SA, Lee PAB, Goldman ER, Anderson GP (2013) Comparison of single domain antibody immobilization strategies evaluated by surface plasmon resonance. J Immunol Methods 388(1–2):68–77. doi:10.1016/j.jim.2012.11.014

25. Walper SA, Lee PAB, Anderson GP, Goldman ER (2013) Selection and characterization of single domain antibodies specific for Bacillus anthracis spore proteins. Antibodies 2:152–167

26. Turner KB, Zabetakis D, Legler P, Goldman ER, Anderson GP (2014) Isolation and epitope mapping of staphylococcal enterotoxin B single-domain antibodies. Sensors 14(6):10846–10863. doi:10.3390/s140610846

27. Anderson G, Liu J, Hale M, Bernstein R, Moore M, Swain M, Goldman E (2008) Development of antiricin single domain antibodies toward detection and therapeutic reagents. Anal Chem 80(24):9604–9611. doi:10.1021/ac8019398

28. Anderson G, Bernstein R, Swain M, Zabetakis D, Goldman E (2010) Binding kinetics of antiricin single domain antibodies and improved detection using a B chain specific binder. Anal Chem 82(17):7202–7207. doi:10.1021/ac100961x

29. Raphael MP, Christodoulides JA, Mulvaney SP, Miller MM, Long JP, Byers JM (2012) A new methodology for quantitative LSPR

biosensing and imaging. Anal Chem 84(3):1367–1373. doi:10.1021/ac2023266

30. Goldman ER, Brozozog-Lee PA, Zabetakis D, Turner KB, Walper SA, Liu JL, Anderson GP (2014) Negative tail fusions can improve ruggedness of single domain antibodies. Protein Expr Purif 95:226–232. doi:10.1016/j.pep.2014.01.003

31. Oshea EK, Lumb KJ, Kim PS (1993) Peptide velcro—design of a heterodimeric coiled-coil. Curr Biol 3(10):658–667. doi:10.1016/0960-9822(93)90063-t

32. Goldman ER, Anderson GP, Brozozog-Lee PA, Zabetakis D (2013) SdAb heterodimer formation using leucine zippers. In: Conference on Sensing Technologies for Global Health, Military Medicine, and Environmental Monitoring III, Baltimore, MD, Apr 29-May 01 2013. Proceedings of SPIE 8723. Spie-Int Soc Optical Engineering, BELLINGHAM. doi:10.1117/12.2016145

33. Liu JL, Zabetakis D, Walper SA, Goldman ER, Anderson GP (2014) Bioconjugates of rhizavidin with single domain antibodies as bifunctional immunoreagents. J Immunol Methods 411:37–42. doi:10.1016/j.jim.2014.06.004

34. Raphael MP, Christodoulides JA, Delehanty JB, Long JP, Pehrsson PE, Byers JM (2013) Quantitative LSPR imaging for biosensing with single nanostructure resolution. Biophys J 104(1):30–36. doi:10.1016/j.bpj.2012.11.3821

35. Stenberg E, Persson B, Roos H, Urbaniczky C (1991) Quantitative-determination of surface concentration of protein with surface-plasmon resonance using radiolableled proteins. J Colloid Interface Sci 143(2):513–526. doi:10.1016/0021-9797(91)90284-f